ACS NANO

www.acsnano.org

ARTICLE

Highly Oriented Atomically Thin Ambipolar $MoSe_2$ Grown by Molecular Beam Epitaxy

Ming-Wei Chen,[†,‡] Dmitry Ovchinnikov,[†,‡] Sorin Lazar,[§] Michele Pizzochero,[∥] Michael Brian Whitwick,[†] Alessandro Surrente,[⊥] Michał Baranowski,[⊥,#] Oriol Lopez Sanchez,[†,‡] Philippe Gillet,[∥] Paulina Plochocka,[⊥] Oleg V. Yazyev,[∥] and Andras Kis*[,†,‡]

[†]Electrical Engineering Institute, École Polytechnique Fédérale de Lausanne (EPFL), CH-1015 Lausanne, Switzerland

[‡]Institute of Materials Science and Engineering, École Polytechnique Fédérale de Lausanne (EPFL), CH-1015 Lausanne, Switzerland

[§]FEI Electron Optics, 5600 KA Eindhoven, The Netherlands

[∥]Institute of Physics, École Polytechnique Fédérale de Lausanne (EPFL), CH-1015 Lausanne, Switzerland

[⊥]Laboratoire National des Champs Magnétiques Intenses CNRS-UGA-UPS-INSA, 143 avenue de Rangueil, 31400 Toulouse, France

[#]Department of Experimental Physics, Faculty of Fundamental Problems of Technology, Wrocław University of Science and Technology, Wybrzeze Wyspianskiego 27, 50-370 Wrocław, Poland

Supporting Information

ABSTRACT: **Transition metal dichalcogenides (TMDCs), together with other two-dimensional (2D) materials, have attracted great interest due to the unique optical and electrical properties of atomically thin layers. In order to fulfill their potential, developing large-area growth and understanding the properties of TMDCs have become crucial. Here, we have used molecular beam epitaxy (MBE) to grow atomically thin $MoSe_2$ on GaAs(111)B. No intermediate compounds were detected at the interface of as-grown films. Careful optimization of the growth temperature can result in the growth of highly aligned films with only two possible crystalline orientations due to broken inversion symmetry. As-grown films can be transferred onto insulating substrates, allowing their optical and electrical properties to be probed. By using polymer electrolyte gating, we have achieved ambipolar transport in MBE-grown $MoSe_2$. The temperature-dependent transport characteristics can be explained by the 2D variable-range hopping (2D-VRH) model, indicating that the transport is strongly limited by the disorder in the film.**

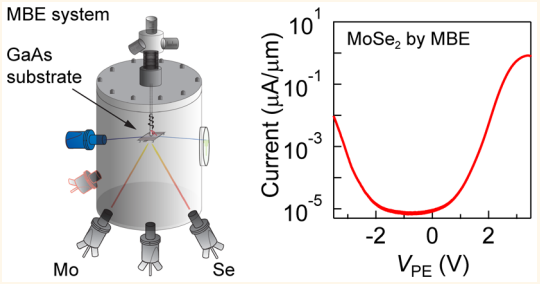

KEYWORDS: *two-dimensional materials, two-dimensional semiconductors, $MoSe_2$, epitaxial growth, ambipolar electrical transport, transmission electron microscopy*

Atomically thin two-dimensional (2D) materials have shown great potential because of their interesting electrical and optical properties.[1−4] Potential applications in flexible electronics and the possibility to further extend their range of applications by integrating them into heterostructures[5] motivate scientists to develop a reliable way to grow large-area 2D materials.[6−9] Whereas chemical vapor deposition (CVD) can on one hand result in high-quality 2D materials and 2D heterostructures with sharp and clean interfaces,[10] the toxicity of some of the precursors introduces challenges, and the lack of *in situ* characterization and monitoring during growth can lead to nonreproducible results. On the other hand, using molecular beam epitaxy (MBE) to grow atomically thin transition metal dichalcogenides (TMDCs) and other 2D materials *via* van der Waals epitaxy[11−16] has several potential advantages. The deposition can be well controlled using high-purity elemental sources; direct heterostructure growth can be achieved, and the growth in an ultrahigh vacuum environment limits the amount of impurity atoms. In addition, the quality of the MBE-grown film can be monitored during growth *in situ* using reflection high-energy electron diffraction (RHEED). The growth of different TMDCs on various substrates has been recently demonstrated,[17−19] and the band structures and thin film morphology have been intensively investigated using angle-resolved photoemission spectroscopy and scanning tunneling microscopy.[20−22] However, reports on the electrical properties of atomically thin layers grown by MBE[23] are rare and indicate that the material quality needs to be improved further. Starting from this point, it is crucial to optimize epitaxial growth and to

Received: April 19, 2017
Accepted: May 22, 2017
Published: May 22, 2017

DOI: 10.1021/acsnano.7b02726
ACS Nano 2017, 11, 6355−6361

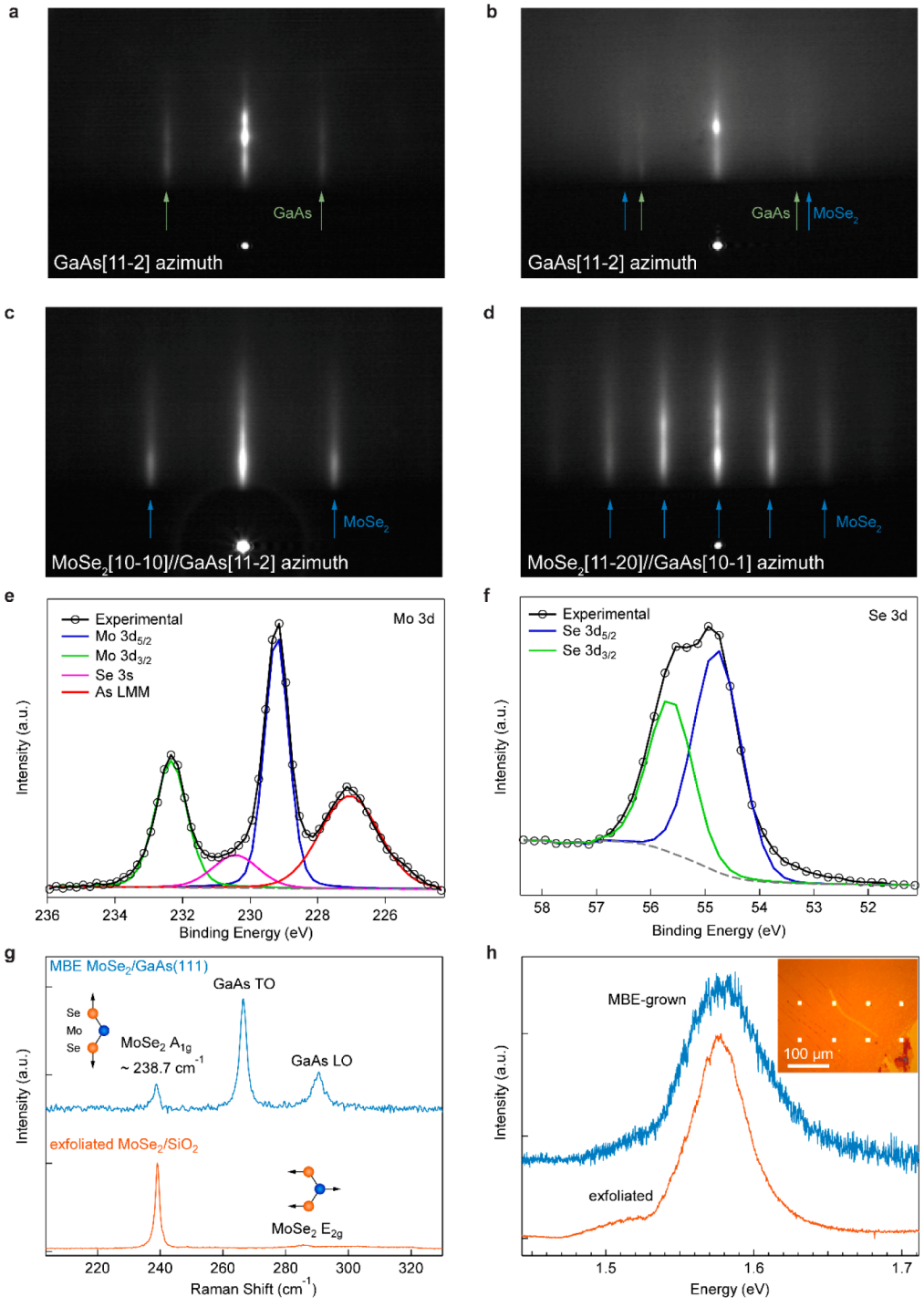

Figure 1. Growth of atomically thin $MoSe_2$ by MBE. (a) RHEED patterns of GaAs(111) along the GaAs[11−2] azimuth at growth start. (b) Half−half transition along the GaAs[11−2] azimuth. (c,d) Nominal monolayer (ML) $MoSe_2$ observed along $MoSe_2$[10−10] and $MoSe_2$[11−20] azimuths at growth end after 22 min. (e) Mo 3d and (f) Se 3d core-level spectra in XPS. (g) Comparison of Raman spectra from MBE-grown and exfoliated ML $MoSe_2$. (h) Photoluminescence of transferred ML $MoSe_2$ and exfoliated ML $MoSe_2$. Inset shows optical image of the transferred film. The sample was grown at 470 °C.

investigate the optical and electrical properties of MBE-grown atomically thin TMDCs.

RESULTS

Here, we report on the use of MBE to grow atomically thin $MoSe_2$ on GaAs(111)B down to nominal monolayer (ML) thickness, exhibiting high optical quality confirmed by photoluminescence (PL) and Raman spectroscopy. We find that using GaAs(111)B as the growth substrate results in a high degree of control over lattice orientation of the domains forming the polycrystalline film. The features of van der Waals epitaxy were thoroughly investigated by X-ray photoelectron spectroscopy (XPS). Using scanning transmission electron microscopy (STEM), we have observed that depending on the growth temperature, polycrystalline $MoSe_2$ films can be composed of grains with either a 15° or a 60° misorientation

DOI: 10.1021/acsnano.7b02726
ACS Nano 2017, 11, 6355−6361

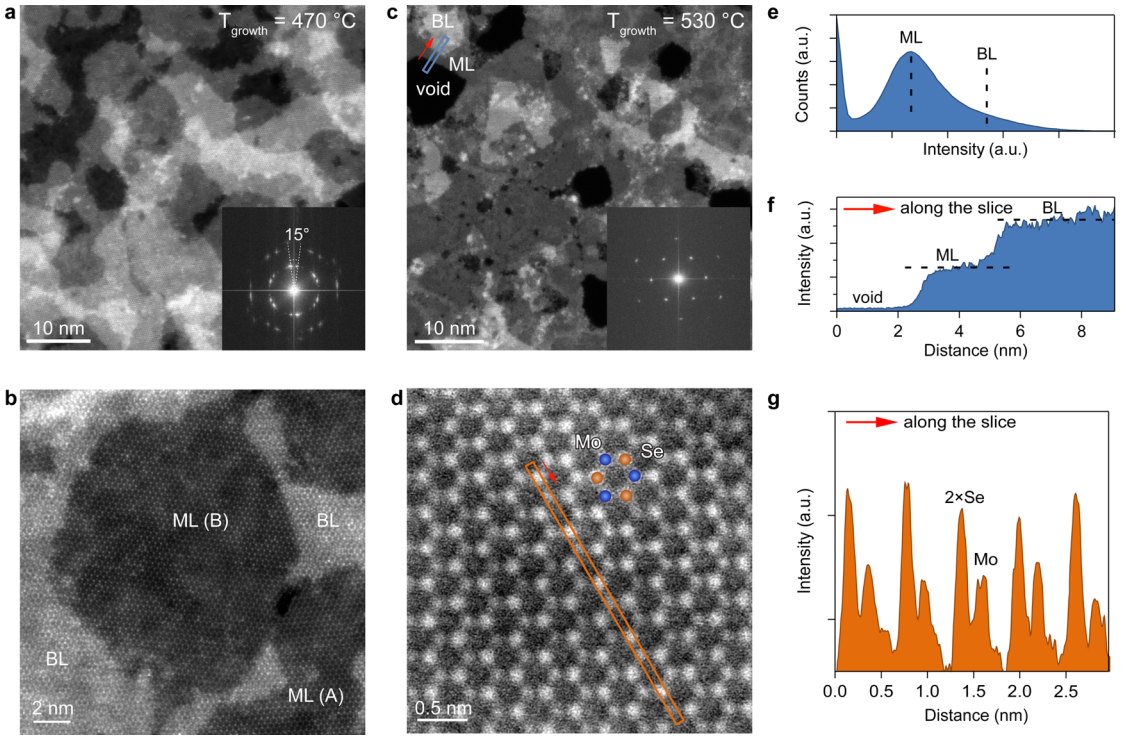

Figure 2. Morphology of MBE-grown $MoSe_2$ films. (a) Low-magnification HAADF-STEM image of $MoSe_2$ grown at 470 °C. Inset is the corresponding FFT image showing two sets of spots. (b) High-magnification image of an incomplete bilayer (BL) composed of ML domains with two orientations denoted as ML(A) and ML(B). (c) Low-magnification HAADF-STEM image of $MoSe_2$ grown at 530 °C. Inset shows the corresponding FFT image with a single set of diffraction patterns. (d) High-magnification image of the ML region with a schematic of atom positions. Bright spots correspond to double Se atoms. (e) Intensity histogram of the image shown in (c). (f) Intensity profile along the slice shown in (c). (g) Intensity profile of the slice from (d).

angle. Both configurations are predicted to be energetically stable by density functional theory (DFT) calculations. We further address the electrical properties of highly oriented nominal ML $MoSe_2$ and demonstrate ambipolar transport behavior using polymer electrolyte gating. Temperature-dependent measurements indicate that the transport is limited by the disorder and can be explained using the 2D variable-range hopping (2D-VRH) model.

Atomically thin $MoSe_2$ films were grown on GaAs(111)B substrates by MBE, and the growth was monitored *in situ* using a RHEED camera. Atomic hydrogen was used to effectively remove native oxide at low temperature without As desorption,[24,25] and a clean GaAs(111)B surface with sharp RHEED streaks along the GaAs[11−2] azimuth was observed (see Figure 1a). As the growth progresses, GaAs-related streaks gradually fade out and are replaced by a new set of faint streaks with a smaller spacing, indicating the formation of $MoSe_2$. A RHEED pattern from the $MoSe_2$ film with a half-layer coverage is shown on Figure 1b, with GaAs and $MoSe_2$ streaks having similar intensities. GaAs-related streaks completely vanish as a full film is grown, while $MoSe_2$ streaks become more intense Figure 1c. The sharp streaks in Figure 1c,d indicate the epitaxy with $MoSe_2$[10−10]//GaAs[11−2] and $MoSe_2$[11−20]//GaAs[10−1], respectively. The van der Waals epitaxy thus provides a reliable way for developing large-scale 2D materials on different substrates.[19,26]

Films grown on GaAs(111)B were examined *ex situ* using X-ray photoelectron spectroscopy (XPS). Figure 1e shows the core-level spectrum of the Mo 3d range. The binding energies of Mo $3d_{5/2}$ and Mo $3d_{3/2}$ peaks are 229.2 and 232.4 eV, respectively. An additional As_{LMM} peak with a lower binding energy of 227.2 eV is also observed. The Se 3d core-level spectrum in Figure 1f shows an Se $3d_{5/2}$ peak at 54.9 eV and an Se $3d_{3/2}$ peak at 55.8 eV, demonstrating the existence of Mo−Se bonds. A consistent binding energy shift is observed in the core-level spectra of Ga 3d and As 3d between pristine GaAs substrate and as-grown $MoSe_2$, implying that charge transfer takes place at the interface (see Supplementary Section 1 for more details). On the other hand, the peak positions and the high quality of fitting show that no intermediate compounds exist at the interface, as expected from van der Waals epitaxy.

The Raman spectrum of nominal ML $MoSe_2$/GaAs(111) shown on Figure 1g clearly shows the $MoSe_2$ A_{1g} mode at 238.7 cm^{-1}, which is comparable with that of exfoliated ML $MoSe_2$ on 270 nm SiO_2. Photoluminescence spectroscopy was also used to investigate the optical properties of ML $MoSe_2$. In order to avoid the optical quenching effect from the substrate,[18,27] the as-grown film was transferred onto a 270 nm SiO_2/Si chip, with the optical image shown in the inset of Figure 1h and Figure S2. The 1.58 eV peak recorded at room temperature is clearly shown in Figure 1h and is comparable with the exfoliated ML flake in terms of the peak positon. Despite inevitable existence of wrinkles and folded regions due to the imperfect transfer process which might introduce defects and peak broadening, the full width at half-maximum (fwhm) of 37 meV is comparable to that of exfoliated ML flakes (fwhm = 27 meV).

The films were transferred onto the TEM grids and investigated using Cs-corrected STEM in order to examine their morphology. Figure 2a shows a low-magnification high-angle annular dark-field (HAADF)-STEM image of $MoSe_2$ grown at the temperature of 470 °C. The patch-like islands

DOI: 10.1021/acsnano.7b02726
ACS Nano 2017, 11, 6355−6361

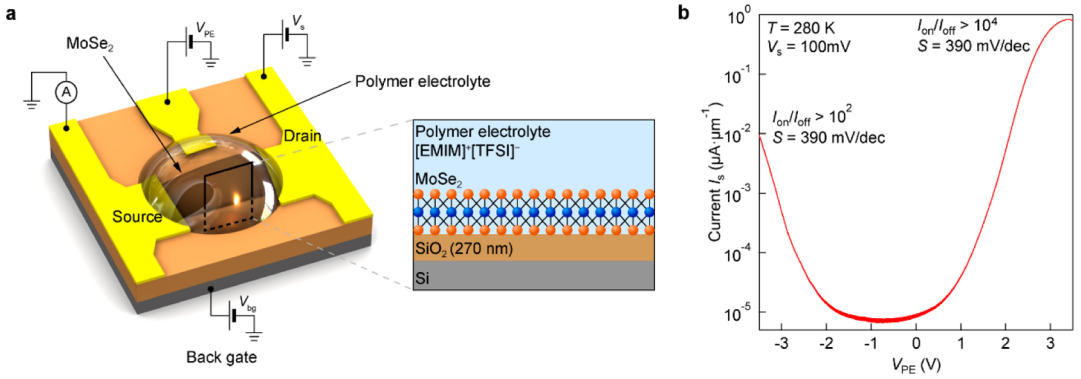

Figure 3. Ambipolar transport in $MoSe_2$ EDLT. (a) Schematic of the $MoSe_2$ EDLT in a dual-gate geometry. The back gate is used to modulate the charge density in the 2D channel around the value set by the reference electrode with the applied voltage V_{PE}. (b) Channel current as a function of V_{PE} showing ambipolar behavior.

with a typical size of a few nm with different brightness represent regions with varying thicknesses. Surprisingly, the corresponding fast Fourier transform (FFT) image calculated from this image and shown in the inset of Figure 2a shows only two sets of spots with a six-fold symmetry, rotated by ∼15° with respect to each other. The high-magnification HAADF-STEM image in Figure 2b shows corresponding domains with a relative rotation of 15°, labeled ML(A) and ML(B). These are sometimes also stacked on top of each other, forming bilayers (BLs). A more detailed analysis of the grain orientation is presented on Figure S3 and shows that both orientations appear with roughly the same frequency in the ML film. Most of the BL area (∼70%) is, however, of the ML(A) + ML(B) type, composed of two $MoSe_2$ layers with an interlayer twist of 15° and could present an interesting material system for studying the effect of interlayer twist on electrical and optical properties of 2D semiconductors.[28]

We have gained further insight into the stability of both types of $MoSe_2$/GaAs(111)B superlattices by considering several models and determining their formation energies through DFT calculations (see Supplementary Section 3). The picture that emerges suggests that a twisting angle not only dramatically reduces the strain in the $MoSe_2$ lattice but also leads to a slightly more favorable interaction with the GaAs(111)B substrate, irrespectively of the relative $MoSe_2$−GaAs orientation. Overall, formation energies of oriented and misoriented $MoSe_2$/GaAs(111)B superlattices are very similar, indicating that both cases are likely to form. Nevertheless, it is also worth mentioning that the growth dynamics should also play a role in the migration of adatoms prior to in-plane bond formation, which could influence the growth, resulting in large regions with single orientation. Possible changes in the surface reconstruction at these temperatures close to GaAs decomposition are not taken into account either, which could explain the difference in the morphology of films grown at these two temperatures.

A slight increase of growth temperature, into the 500−530 °C range, results in increased order in the film, with the grains no longer showing the 15° misorientation. The HAADF-STEM image of the film is shown on Figure 2c. The corresponding FFT image now shows only one set of peaks. Since ML $MoSe_2$ does not possess inversion symmetry, we cannot exclude the presence of grains with a 60° relative orientation at this point as these would result in a set of diffraction peaks at the same positions in Fourier space. The presence of voids in the film indicates that BLs start to form before the first MLs complete. Similar morphologies of MBE-grown $MoSe_2$ on highly oriented pyrolytic graphite, graphene, and SiC(0001) were also observed by STM by other groups.[18,21,27,29,30]

Because the intensities recorded in HAADF-STEM images are related to Rutherford scattering, which increases with the atomic number (Z),[31,32] different intensities in the image can be attributed to different layer thickness. Figure 2b shows the intensity histogram with dashed lines that correspond to intensities in ML and BL regions. The intensity profile along the slice of interest is plotted in Figure 2c, showing the thickness varying from ML to BL. Figure 2d shows a high-magnification image of a ML region with the intensity profile along a slice of interest shown in Figure 2f, where the positions of Mo and Se atoms can be assigned to periodically varying intensities. The ML has a 2H structure with a lattice constant estimated to be 3.29 ± 0.03 nm, which is in line with the bulk lattice constants reported in literature.[33,34]

To further confirm the long-range uniformity of the $MoSe_2$ film, we have measured second harmonic generation (SHG) from as-grown $MoSe_2$/GaAs(111)B and suspended $MoSe_2$ on TEM grids (Figure S7). Polar plots of SHG intensity show six-fold symmetry, whereas the PL intensity and Raman A_{1g} peak position and intensity maps indicate a high degree of uniformity (see Supplementary Section 4).

We now focus on the electrical properties of 0 and 60° $MoSe_2$ with nominal ML thickness. We use electric double-layer transistors (EDLT) in order to access a wide range of electrostatically induced doping levels and to reduce Schottky barrier heights at contacts, allowing efficient electron and hole injection using the same contact material.[35] Figure 3 shows the schematic of the device. The polymer electrolyte PS−PMMA-PS:[EMIM]-[TFSI] is spin-coated on top. It allows us to reach high carrier densities and increases the efficiency of carrier injection, making it ideal for achieving ambipolar regime of operation.[35,36] We also include a back gate, allowing charge carrier modulation in the semiconducting film at temperatures below the freezing point of the polymer electrolyte (T ∼ 200 K). Devices without a polymer electrolyte show a very poor transistor behavior (see Supplementary Section 5). The dependence of the EDLT on the polymer electrolyte voltage V_{PE} exhibits a clear ambipolar behavior close to room temperature (T = 280 K) (Figure 3b). We find a current I_{on}/I_{off} ratio of ∼10^4 and ∼10^2 for the n and p sides, respectively. The maximum current density on the n side, with the value of ∼1 μA/μm, is 2 orders of magnitude larger than that on the p side, possibly due to intervalley scattering of electrons, while

DOI: 10.1021/acsnano.7b02726
ACS Nano 2017, 11, 6355−6361

the off current remains at pA levels. The subthreshold swing calculated from the linear region is ~390 mV/dec for both sides. Field-effect mobilities can be extracted from four-contact devices by freezing the polymer electrolyte at 200 K and performing a back-gate sweep (see Supplementary Section 6), which allows the charge carrier concentration in the 2D semiconductor to be modulated around the value set by V_{PE} prior to freezing the electrolyte. The extracted electron mobility μ_e is ~0.05 $cm^2 V^{-1} s^{-1}$, and hole mobility μ_h is ~0.28 $cm^2 V^{-1} s^{-1}$. The mobility values are significantly lower than those of CVD-grown $MoSe_2$.[37,38] These results indicate that charge carrier transport is strongly influenced by the disorder in the film.[23,39]

In order to elucidate the dominant transport mechanism in MBE-grown atomically thin $MoSe_2$, we have performed electrical measurements as a function of temperature, polymer electrolyte, and back-gate voltage. Figure 4a shows the sheet conductivity G_{sh} as a function of V_{PE} based on the four-contact device shown in the inset. The V_{PE} applied for the p side needs to be pushed to $V_{PE} < -4$ V to reach the same value as on G_{sh} of the n side, indicating strong electron doping or Fermi level pinning to the conduction band. A drop in G_{sh} takes place at $V_{PE} > 3$ V and can be attributed to the electrolyte-induced disorder which is commonly observed in experiments involving EDLTs.[40,41] The sweep at 280 K can then provide a reference curve for different doping levels that can be achieved by changing V_{PE}. Once the doping level at a given V_{PE} is stabilized at 280 K, we freeze the electrolyte down to 200 K with a cool-down rate of 1 K/min. The V_{PE} is then disconnected at 200 K after the electrolyte was completely frozen so that G_{sh} can be stabilized (see Supplementary Section 7). The G_{sh} during each cool down was recorded down to 12 K with a cooling rate of 0.5 °C/min. The process was reversible after a mild annealing by ramping the temperature to 333 K.

The G_{sh} of $MoSe_2$ at a given V_{PE} monotonically decreases with decreasing temperature, showing semiconducting behavior for both sides. The dependence above 80 K follows the 2D-VRH model[42] with the relation $G_{sh} \propto \exp[-(T_0/T)^{1/3}]$, where T_0 is the characteristic temperature. A linear fit of ln G_{sh} to $T^{-1/3}$ is plotted at each given V_{PE}, demonstrating the validity of the 2D-VRH mechanism for both sides (Figure 4b,c). The VRH mechanism is usually observed in disorded systems,[23,40] and the results imply that the transport of $MoSe_2$ EDLT is strongly influenced by the voids and the nanometer-scale grains in the film.

Charge carriers are strongly scattered and tend to hop between different conductive paths. The localization length can be changed in a small range by changing V_{PE}, that is, changing the doping level. The dependency is evident by extracting T_0 from the fits to the 2D-VRH model with the value of slopes s extracted from Figure 4b,c, where $T_0 = s^3$. The values of T_0 decrease by more than 1 order of magnitude with the increase of $|V_{PE}|$ because of the increase of carrier densities in the material, thus screening the disorder along the conductive paths. The localization length ξ_{loc} can be extracted using the expression $\xi_{loc} = \sqrt{13.8/k_B D T_0}$, where k_B is the Boltzmann constant and D the density of states (see Supplementary Section 8). The results are plotted in Figure 4d,e for p and n sides, respectively. Holes have a slightly lower ξ_{loc}, with ξ_{loc} reaching a maximum value of ~4 nm at $V_{PE} = -4.2$ V. The n side, on the other hand, shows tunable ξ_{loc} up to ~9 nm with $V_{PE} = 2.45$ V. All values of ξ_{loc} have the same order of magnitude as the grain size shown in STEM images, indicating that the 2D-VRH transport is linked to the disorder in the as-grown $MoSe_2$. Future MBE-based growth efforts will have to concentrate on increasing the grain size in order to improve the film quality.

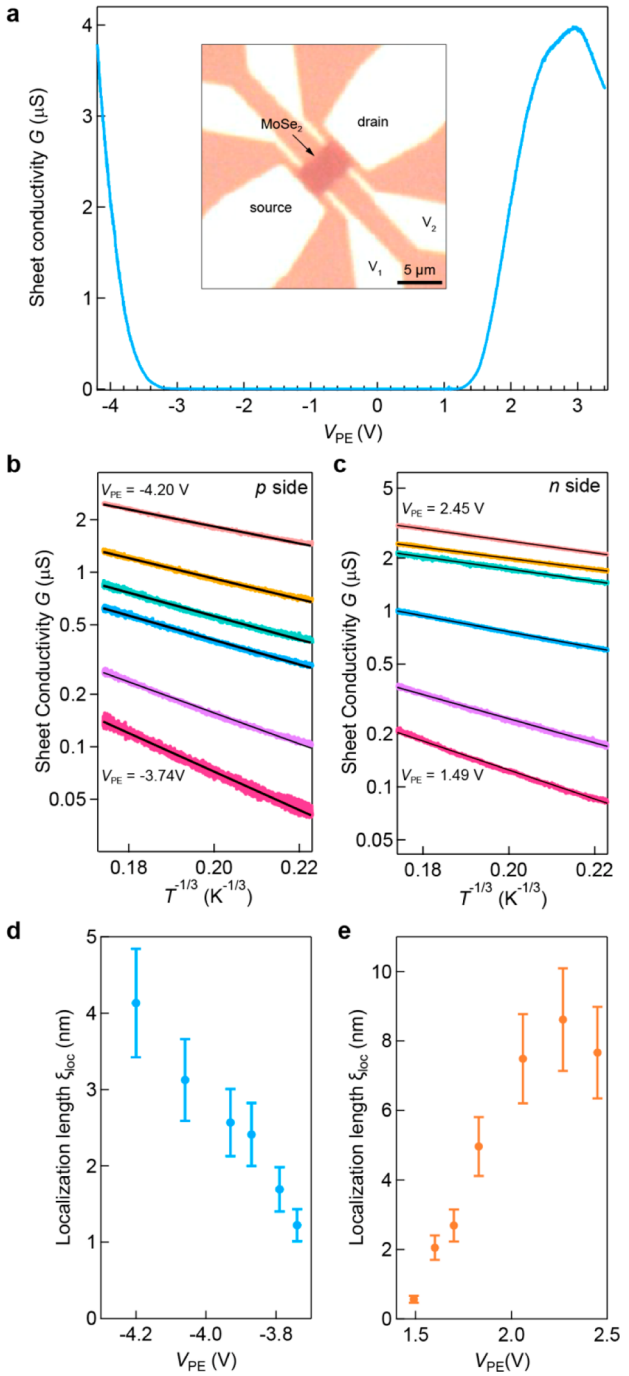

Figure 4. Two-dimensional VRH transport mechanism in $MoSe_2$ EDLT. (a) Sheet conductivity G_{sh} as a function of V_{PE} at 280 K. Inset: Optical image of the four-contact device. (b,c) G_{sh} as a function of $T^{-1/3}$ on the hole and electron sides for different values of V_{PE} filled lines corresponds to fits to the VRH model. (d) Evolution of the localization length ξ_{loc} with V_{PE}, extracted from fits to the VRH model on the hole branch. (e) Dependence of ξ_{loc} on V_{PE} for the electron branch.

DOI: 10.1021/acsnano.7b02726
ACS Nano 2017, 11, 6355−6361

CONCLUSION

In conclusion, we have grown atomically thin $MoSe_2$ using MBE. Films show a high degree of alignment due to the van der Waals interaction with the GaAs substrate and can be transferred to insulating substrates for further optical and electrical transport studies. We realize electrolytically gated transistors based on transferred ML $MoSe_2$ films. Electrical transport follows the 2D-VRH model due to disorder in the film, with localization length comparable to the grain size.

METHODS

MBE Setup and Material Growth. The growth was carried out in an Omicron MBE (Lab 10) with a $\sim 10^{-10}$ mbar base pressure. Cleaved 1 × 1 cm^2 GaAs(111)B substrates were outgassed at up to 500 °C for at least 30 min. The native oxide was removed from the surface of GaAs(111)B by heating it to 350 °C under a flux of atomic hydrogen. Hydrogen molecules were dissociated by a tungsten filament with Joule heating at 70 W and were introduced into the chamber *via* a leak valve. The procedure lasted 30 min or more at base pressure of $\sim 3 \times 10^{-7}$ mbar, resulting in sharp streaks in RHEED. A Kundsen cell and an electron beam source (EFM-3 from Omicron) were used for Se and Mo evaporation, respectively. The flux rates were calibrated using a quartz crystal microbalance, and the flux ratio of Se/Mo was optimized to be ∼40 for growth. A RHEED camera (Staib Co.) was used to monitor the growth *in situ*. The growth temperature was optimized in the 470−530 °C temperature range. Post-annealing at up to 550 °C was performed in Se atmosphere. Higher temperature leads to GaAs decomposition and increased surface roughness.

XPS and Raman Spectroscopy. The XPS spectra were obtained *ex situ* in a commercial KRATOS AXIS ULTRA system, and a C 1s core-level peak at 284.8 eV was used for the reference. Peak identification and fitting were performed in PHI MultiPak processing software. Raman analysis was performed using a Horiba LabRAM HR800 system using a 532 nm wavelength green laser with spot size ∼4 μm. The laser power was kept below 4 mW during all measurements. We used an 1800 lines/mm grating and have calibrated the system using the polycrystalline Si peak at 520 cm^{-1}. The PL was measured in a home-built setup using a 488 nm laser (Coherent) for excitation.

STEM Microscopy and Analysis. The STEM experiments were performed on a FEI Titan Themis 300 double Cs-corrected microscope at an acceleration voltage of 80 kV in order to minimize beam damage. The scanning probe had a 28 mrad semiconvergence angle, resulting in a resolution close to 1 Å. The data were acquired under annular dark-field conditions using an annular detector with a collection half-angle between 40 and 200 mrad.

Material Transfer and Device Fabrication. As-grown films were coated with PMMA and immersed into 30% $KOH_{(aq)}$ at 90 °C. The detached PMMA layer with the as-grown film was then transferred to a beaker with deionized water several times to remove excess $KOH_{(aq)}$ and was transferred onto a degenerately doped n^{++} Si chip covered by 270 nm SiO_2 or TEM grids. PMMA was removed in acetone. Palladium was used for electrical contacts in a standard PMMA-based e-beam lithography process. A second e-beam lithography was performed, followed by O_2/SF_6 plasma etching in order to define the device geometry. To fabricate an EDLT, the PS−PMMA-PS:[EMIM]-[TFSI] electrolyte was spin-coated onto the device and soft-baked at 60 °C for 10 min. A more detailed description is available elsewhere.[43,44] Electrical measurements were carried out using an Agilent 5270B SMU and Keithley 2000 DMM. Cryogenic measurements were performed in a Janis closed-cycle cryogen-free cryostat.

ASSOCIATED CONTENT

Supporting Information

The Supporting Information is available free of charge on the ACS Publications website at DOI: 10.1021/acsnano.7b02726.

Supplementary figures and discussion related to XPS spectroscopy, TEM imaging, DFT calculations, SHG and Raman mapping, field-effect transistor characterization, and variable-range hopping transport mechanism (PDF)

AUTHOR INFORMATION

Corresponding Author

*E-mail: andras.kis@epfl.ch.

ORCID

Paulina Plochocka: 0000-0002-4019-6138

Andras Kis: 0000-0002-3426-7702

Notes

The authors declare no competing financial interest.

ACKNOWLEDGMENTS

We thank R. Gaal for technical assistance with the Raman setup, D. Alexander (CIME) for support with electron microscopy, and P. Mettraux for help with the XPS setup and experiments. We thank D. Dumcenco, H. Kim, and A. Pulkin for fruitful discussions. This work was financially supported by the European Research Council Grant Nos. 240076 and 306504, the Swiss National Science Foundation Grant Nos. 153298 and 162612, funding from the BLAPHENE project under IDEX program Emergence and Programme Investissements d'Avenir under the program ANR-11-IDEX-0002-02, reference ANR-10-LABX-0037-NEXT. This work was financially supported by funding from the European Union's Seventh Framework Programme FP7/2007-2013 under Grant Agreement No. 318804 (SNM.) and was carried out in frames of the Marie Curie ITN network "MoWSeS" (Grant No. 317451). We acknowledge funding by the EC under the Graphene Flagship (Grant Agreement No. 604391). First-principles calculations were performed at the Swiss National Supercomputing Centre (CSCS) under the project s-675.

REFERENCES

(1) Radisavljevic, B.; Radenovic, A.; Brivio, J.; Giacometti, V.; Kis, A. Single-Layer MoS_2 Transistors. *Nat. Nanotechnol.* **2011**, *6*, 147−150.

(2) Splendiani, A.; Sun, L.; Zhang, Y.; Li, T.; Kim, J.; Chim, C.-Y.; Galli, G.; Wang, F. Emerging Photoluminescence in Monolayer MoS_2. *Nano Lett.* **2010**, *10*, 1271−1275.

(3) Mak, K. F.; Lee, C.; Hone, J.; Shan, J.; Heinz, T. F. Atomically Thin MoS_2: A New Direct-Gap Semiconductor. *Phys. Rev. Lett.* **2010**, *105*, 136805.

(4) Wang, Q. H.; Kalantar-Zadeh, K.; Kis, A.; Coleman, J. N.; Strano, M. S. Electronics and Optoelectronics of Two-Dimensional Transition Metal Dichalcogenides. *Nat. Nanotechnol.* **2012**, *7*, 699−712.

(5) Geim, A. K.; Grigorieva, I. V. Van Der Waals Heterostructures. *Nature* **2013**, *499*, 419−425.

(6) Liu, K.-K.; Zhang, W.; Lee, Y.-H.; Lin, Y.-C.; Chang, M.-T.; Su, C.-Y.; Chang, C.-S.; Li, H.; Shi, Y.; Zhang, H.; et al. Growth of Large-Area and Highly Crystalline MoS_2 Thin Layers on Insulating Substrates. *Nano Lett.* **2012**, *12*, 1538−1544.

(7) Najmaei, S.; Liu, Z.; Zhou, W.; Zou, X.; Shi, G.; Lei, S.; Yakobson, B. I.; Idrobo, J.-C.; Ajayan, P. M.; Lou, J. Vapor Phase Growth and Grain Boundary Structure of Molybdenum Disulfide Atomic Layers. *Nat. Mater.* **2013**, *12*, 754−759.

(8) van der Zande, A. M.; Huang, P. Y.; Chenet, D. A.; Berkelbach, T. C.; You, Y.; Lee, G.-H.; Heinz, T. F.; Reichman, D. R.; Muller, D. A.; Hone, J. C. Grains and Grain Boundaries in Highly Crystalline Monolayer Molybdenum Disulphide. *Nat. Mater.* **2013**, *12*, 554−561.

(9) Dumcenco, D.; Ovchinnikov, D.; Marinov, K.; Lazić, P.; Gibertini, M.; Marzari, N.; Sanchez, O. L.; Kung, Y.-C.; Krasnozhon,

DOI: 10.1021/acsnano.7b02726
ACS Nano 2017, 11, 6355−6361

D.; Chen, M.-W.; et al. Large-Area Epitaxial Monolayer MoS_2. *ACS Nano* **2015**, *9*, 4611−4620.
(10) Li, M.-Y.; Shi, Y.; Cheng, C.-C.; Lu, L.-S.; Lin, Y.-C.; Tang, H.-L.; Tsai, M.-L.; Chu, C.-W.; Wei, K.-H.; He, J.-H.; et al. Epitaxial Growth of a Monolayer WSe_2-MoS_2 Lateral p-n Junction with an Atomically Sharp Interface. *Science* **2015**, *349*, 524−528.
(11) Koma, A. Van Der Waals Epitaxy for Highly Lattice-Mismatched Systems. *J. Cryst. Growth* **1999**, *201*−*202*, 236−241.
(12) Koma, A. Van Der Waals Epitaxy—a New Epitaxial Growth Method for a Highly Lattice-Mismatched System. *Thin Solid Films* **1992**, *216*, 72−76.
(13) Koma, A.; Yoshimura, K. Ultrasharp Interfaces Grown with Van Der Waals Epitaxy. *Surf. Sci.* **1986**, *174*, 556−560.
(14) Schlaf, R.; Tiefenbacher, S.; Lang, O.; Pettenkofer, C.; Jaegermann, W. Van Der Waals Epitaxy of Thin InSe Films on $MoTe_2$. *Surf. Sci.* **1994**, *303*, L343−L347.
(15) Lang, O.; Schlaf, R.; Tomm, Y.; Pettenkofer, C.; Jaegermann, W. Single Crystalline GaSe/WSe_2 Heterointerfaces Grown by van Der Waals Epitaxy. I. Growth Conditions. *J. Appl. Phys.* **1994**, *75*, 7805−7813.
(16) Schlaf, R.; Pettenkofer, C.; Jaegermann, W. Band Lineup of a SnS2/SnSe2/SnS2 Semiconductor Quantum Well Structure Prepared by van Der Waals Epitaxy. *J. Appl. Phys.* **1999**, *85*, 6550−6556.
(17) Lehtinen, O.; Komsa, H.-P.; Pulkin, A.; Whitwick, M. B.; Chen, M.-W.; Lehnert, T.; Mohn, M. J.; Yazyev, O. V.; Kis, A.; Kaiser, U.; et al. Atomic Scale Microstructure and Properties of Se-Deficient Two-Dimensional $MoSe_2$. *ACS Nano* **2015**, *9*, 3274−3283.
(18) Vishwanath, S.; Liu, X.; Rouvimov, S.; Mende, P. C.; Azcatl, A.; McDonnell, S.; Wallace, R. M.; Feenstra, R. M.; Furdyna, J. K.; Jena, D.; et al. Comprehensive Structural and Optical Characterization of MBE Grown $MoSe_2$ on Graphite, CaF2 and Graphene. *2D Mater.* **2015**, *2*, 024007.
(19) Xenogiannopoulou, E.; Tsipas, P.; Aretouli, K. E.; Tsoutsou, D.; Giamini, S. A.; Bazioti, C.; Dimitrakopulos, G. P.; Komninou, P.; Brems, S.; Huyghebaert, C.; et al. High-Quality, Large-Area $MoSe_2$ and $MoSe_2$/Bi_2Se_3 Heterostructures on AlN(0001)/Si(111) Substrates by Molecular Beam Epitaxy. *Nanoscale* **2015**, *7*, 7896−7905.
(20) Zhang, Y.; Chang, T.-R.; Zhou, B.; Cui, Y.-T.; Yan, H.; Liu, Z.; Schmitt, F.; Lee, J.; Moore, R.; Chen, Y.; et al. Direct Observation of the Transition from Indirect to Direct Bandgap in Atomically Thin Epitaxial $MoSe_2$. *Nat. Nanotechnol.* **2013**, *9*, 111−115.
(21) Ugeda, M. M.; Bradley, A. J.; Shi, S.-F.; da Jornada, F. H.; Zhang, Y.; Qiu, D. Y.; Ruan, W.; Mo, S.-K.; Hussain, Z.; Shen, Z.-X.; et al. Giant Bandgap Renormalization and Excitonic Effects in a Monolayer Transition Metal Dichalcogenide Semiconductor. *Nat. Mater.* **2014**, *13*, 1091−1095.
(22) Barja, S.; Wickenburg, S.; Liu, Z.-F.; Zhang, Y.; Ryu, H.; Ugeda, M. M.; Hussain, Z.; Shen, Z.-X.; Mo, S.-K.; Wong, E.; et al. Charge Density Wave Order in 1D Mirror Twin Boundaries of Single-Layer $MoSe_2$. *Nat. Phys.* **2016**, *12*, 751−756.
(23) Roy, A.; Movva, H. C. P.; Satpati, B.; Kim, K.; Dey, R.; Rai, A.; Pramanik, T.; Guchhait, S.; Tutuc, E.; Banerjee, S. K. Structural and Electrical Properties of $MoTe_2$ and $MoSe_2$ Grown by Molecular Beam Epitaxy. *ACS Appl. Mater. Interfaces* **2016**, *8*, 7396−7402.
(24) Sugaya, T.; Kawabe, M. Low-Temperature Cleaning of GaAs Substrate by Atomic Hydrogen Irradiation. *Jpn. J. Appl. Phys.* **1991**, *30*, L402.
(25) Khatiri, A.; Krzyzewski, T. J.; McConville, C. F.; Jones, T. S. Atomic Hydrogen Cleaning of Low-Index GaAs Surfaces. *J. Cryst. Growth* **2005**, *282*, 1−6.
(26) Kim, J.; Bayram, C.; Park, H.; Cheng, C.-W.; Dimitrakopoulos, C.; Ott, J. A.; Reuter, K. B.; Bedell, S. W.; Sadana, D. K. Principle of Direct van Der Waals Epitaxy of Single-Crystalline Films on Epitaxial Graphene. *Nat. Commun.* **2014**, *5*, 4836.
(27) Jiao, L.; Liu, H. J.; Chen, J. L.; Yi, Y.; Chen, W. G.; Cai, Y.; Wang, J. N.; Dai, X. Q.; Wang, N.; Ho, W. K.; et al. Molecular-Beam Epitaxy of Monolayer $MoSe_2$: Growth Characteristics and Domain Boundary Formation. *New J. Phys.* **2015**, *17*, 053023.
(28) Liu, K.; Zhang, L.; Cao, T.; Jin, C.; Qiu, D.; Zhou, Q.; Zettl, A.; Yang, P.; Louie, S. G.; Wang, F. Evolution of Interlayer Coupling in Twisted Molybdenum Disulfide Bilayers. *Nat. Commun.* **2014**, *5*, 4966.
(29) Liu, H.; Jiao, L.; Yang, F.; Cai, Y.; Wu, X.; Ho, W.; Gao, C.; Jia, J.; Wang, N.; Fan, H.; et al. Dense Network of One-Dimensional Midgap Metallic Modes in Monolayer $MoSe_2$ and Their Spatial Undulations. *Phys. Rev. Lett.* **2014**, *113*, 066105.
(30) Bradley, A. J.; M. Ugeda, M.; da Jornada, F. H.; Qiu, D. Y.; Ruan, W.; Zhang, Y.; Wickenburg, S.; Riss, A.; Lu, J.; Mo, S.-K.; et al. Probing the Role of Interlayer Coupling and Coulomb Interactions on Electronic Structure in Few-Layer $MoSe_2$ Nanostructures. *Nano Lett.* **2015**, *15*, 2594−2599.
(31) Krivanek, O. L.; Chisholm, M. F.; Nicolosi, V.; Pennycook, T. J.; Corbin, G. J.; Dellby, N.; Murfitt, M. F.; Own, C. S.; Szilagyi, Z. S.; Oxley, M. P.; et al. Atom-by-Atom Structural and Chemical Analysis by Annular Dark-Field Electron Microscopy. *Nature* **2010**, *464*, 571−574.
(32) Hartel, P.; Rose, H.; Dinges, C. Conditions and Reasons for Incoherent Imaging in STEM. *Ultramicroscopy* **1996**, *63*, 93−114.
(33) Ohuchi, F. S.; Parkinson, B. A.; Ueno, K.; Koma, A. Van Der Waals Epitaxial Growth and Characterization of $MoSe_2$ Thin Films on SnS2. *J. Appl. Phys.* **1990**, *68*, 2168−2175.
(34) James, P. B.; Lavik, M. T. The Crystal Structure of $MoSe_2$. *Acta Crystallogr.* **1963**, *16*, 1183−1183.
(35) Allain, A.; Kis, A. Electron and Hole Mobilities in Single-Layer WSe_2. *ACS Nano* **2014**, *8*, 7180−7185.
(36) Zhang, Y. J.; Ye, J. T.; Yomogida, Y.; Takenobu, T.; Iwasa, Y. Formation of a Stable P−n Junction in a Liquid-Gated MoS_2 Ambipolar Transistor. *Nano Lett.* **2013**, *13*, 3023−3028.
(37) Jung, C.; Kim, S. M.; Moon, H.; Han, G.; Kwon, J.; Hong, Y. K.; Omkaram, I.; Yoon, Y.; Kim, S.; Park, J. Highly Crystalline CVD-Grown Multilayer $MoSe_2$ Thin Film Transistor for Fast Photodetector. *Sci. Rep.* **2015**, *5*, 15313.
(38) Wang, X.; Gong, Y.; Shi, G.; Chow, W. L.; Keyshar, K.; Ye, G.; Vajtai, R.; Lou, J.; Liu, Z.; Ringe, E.; et al. Chemical Vapor Deposition Growth of Crystalline Monolayer $MoSe_2$. *ACS Nano* **2014**, *8*, 5125−5131.
(39) Dau, M. T.; Vergnaud, C.; Marty, A.; Rortais, F.; Beigné, C.; Boukari, H.; Bellet-Amalric, E.; Guigoz, V.; Renault, O.; Alvarez, C.; et al. Millimeter-Scale Layered $MoSe_2$ Grown on Sapphire and Evidence for Negative Magnetoresistance. *Appl. Phys. Lett.* **2017**, *110*, 011909.
(40) Ovchinnikov, D.; Gargiulo, F.; Allain, A.; Pasquier, D. J.; Dumcenco, D.; Ho, C.-H.; Yazyev, O. V.; Kis, A. Disorder Engineering and Conductivity Dome in ReS_2 with Electrolyte Gating. *Nat. Commun.* **2016**, *7*, 12391.
(41) Gallagher, P.; Lee, M.; Petach, T. A.; Stanwyck, S. W.; Williams, J. R.; Watanabe, K.; Taniguchi, T.; Goldhaber-Gordon, D. A High-Mobility Electronic System at an Electrolyte-Gated Oxide Surface. *Nat. Commun.* **2015**, *6*, 6437.
(42) Mott, N. F. Conduction in Non-Crystalline Materials. *Philos. Mag.* **1969**, *19*, 835−852.
(43) Yomogida, Y.; Pu, J.; Shimotani, H.; Ono, S.; Hotta, S.; Iwasa, Y.; Takenobu, T. Ambipolar Organic Single-Crystal Transistors Based on Ion Gels. *Adv. Mater.* **2012**, *24*, 4392−4397.
(44) Pu, J.; Yomogida, Y.; Liu, K.-K.; Li, L.-J.; Iwasa, Y.; Takenobu, T. Highly Flexible MoS_2 Thin-Film Transistors with Ion Gel Dielectrics. *Nano Lett.* **2012**, *12*, 4013−4017.

DOI: 10.1021/acsnano.7b02726
ACS Nano 2017, 11, 6355−6361